Nanomed J. 12(2): 238-251, Spring 2025

RESEARCH PAPER

Selenium nanoparticles loaded nanofibers ameliorate cardiac function after acute myocardial infarction in rat MI model

*Safieh Boroumand [1, 2], Parisa Ahmadi [3], Faraz Sigaroodi [2], Mohammad-Mehdi Khani [2], Fatemeh Ghanbari [4], Shahram Rabbani [1], Seyed Hossein Ahmadi Tafti [1], Asieh Heirani-Tabasi [2], Hossein Ghanbari [1, 3]**

[1]*Research Center for Advanced Technologies in Cardiovascular Medicine, Cardiovascular Diseases Research Institute, Tehran University of Medical Sciences, Tehran, Iran*
[2]*Department of Tissue Engineering and Applied Cell Sciences, School of Advanced Technologies in Medicine, Shahid Beheshti University of Medical Sciences, Tehran, Iran*
[3]*Department of Medical Nanotechnology, School of Advanced Technologies in Medicine, Tehran University of Medical Sciences, Tehran, Iran*
[4]*School of Medicine, Tehran University of Medical Sciences, Tehran, Iran*

ABSTRACT

Objective(s): Acute myocardial infarction causes the heart to lose its proper function due to contractile dysfunction within the damaged ischemic cardiac tissue. Different studies have presented various cardiac patches based on different biomaterials to support the infarcted myocardium to recover cardiac function.

Materialsd Methods: In this study, we developed a nanofiber cardiac patch with antioxidant and antibacterial properties. Polycaprolactone (PCL) nanofibers were enriched with chitosan-coated selenium nanoparticles (Cs-SeNPs) using an electrospinning technique.

Results: The PCL/Cs-SeNPs nanofibers, with an average diameter of 648.36±259.19 nm, displayed antioxidant properties in the DPPH assay. Additionally, viable cell count assessment demonstrated the antibacterial effects of PCL/Cs-SeNPs nanofibers against Staphylococcus aureus and Escherichia coli bacteria. MTT assay results revealed improved proliferation for the PCL/Cs-SeNPs nanofibers compared to the PCL nanofibers scaffold, with no significant cell toxicity. The SEM imaging and DAPI/Phalloidin staining supported the improved cell adhesion with well-expanded cytoskeleton of 3T3 cells on PCL/Cs-SeNPs nanofibers. In the rat model of myocardial infarction, improved cardiac function and reduced post-surgical adhesion were observed 28 days after surgery.

Conclusion: The results of this study suggest that the PCL/Cs-SeNPs nanofibers cardiac patch can be considered a potent supportive strategy for myocardial rehabilitation after myocardial infarction.

Keywords: *Chitosan, Myocardial infarction, Nanofibers, Polycaprolactone, Selenium nanoparticles*

How to cite this article
Boroumand S, Ahmadi P, Sigaroodi F, Khani MM, Ghanbari F, Rabbani Sh, Ahmadi Tafti SH, Heirani A, Ghanbari H. Selenium nanoparticles loaded nanofibers ameliorate cardiac function after acute myocardial infarction in rat MI model. Nanomed J. 2025; 12(2): 238-251. DOI: 10.22038/nmj.2024.79242.1950

INTRODUCTION

Myocardial infarction accounts for approximately 13% of all deaths in the global population and is commonly referred to as the leading cause of morbidity and mortality worldwide [1]. Because of the limited regeneration capacity of myocardial tissue, scar formation in the infarcted site leads to dysfunction of electrical signal propagation and loss of contractile capacity, causing heart failure [2-4]. In addition, increased oxidative stress in the infarcted site leads to progressive tissue damage and cardiomyocyte apoptosis [5, 6]. Despite developing treatment strategies to rehabilitate cardiac function, heart transplantation is the only viable therapeutic strategy, particularly in the case of extensive myocardial infarction. However, a shortage of heart donors raises the necessity of alternative strategies [3]. Several therapeutic approaches have been introduced in preclinical and clinical studies to improve myocardial function, such as stem cell therapy, gene therapy, and growth factors, though the in situ stability and targeting of these therapies need to be modified [7]. A cardiac patch is one of

* *Corresponding author: Email: hghanbari@tums.ac.ir*
Note. This manuscript was submitted on April 10, 2024; approved on July 13, 2024

the impellent approaches to improve myocardial function via mechanical support that can be designed also as a carrier vehicle for stem cells, growth factors, and therapeutic pharmaceutics [2]. Previous studies reported that applying a temporary cardiac patch on the infarcted site of the heart can recover the function of the damaged heart [8]. The cardiomyoplasty with a wrap of muscle has been designed to support the infarcted myocardium as a cardiac patch, however, the clinical results have not been reliable [2]. A tissue-engineered cardiac patch can provide proper mechanical support and can be a proper substrate for cell engraftment and small molecule loading [7]. Different kinds of synthetic biomaterials and natural materials along with different fabrication methods have been studied for cardiac patches based on their specific characteristics [2, 9]. Introduced synthetic biomaterials for cardiac patch engineering comprised of polycaprolactone (PCL), poly (glycerol sebacate (PGS), polypyrrole (PPy), polyurethane (PU), polylactic acid (PLA), poly (lactic-co-glycolic) acid (PLGA), polyvinyl alcohol (PVA), while collagen, chitosan (CS), hyaluronic acid, silk fibroin, alginate, gelatin, and decellularized ECMs have been introduced as natural-based materials for cardiac patches [9]. Synthetic biomaterials confront challenges like poor biocompatibility, nevertheless, natural materials confront poor mechanical properties. Desired properties for cardiac patches can be reinforced in hybrid scaffolds of synthetic and natural materials [9]. The PCL polymer as an FDA-approved material for biomedical applications with the desired degradation rate and mechanical properties has been used for different tissue engineering approaches [10] as well as cardiac patch engineering [11-15]. Though PCL has sufficient mechanical properties [9], but lacks other desired properties for cardiac patches such as electrical conductivity with antibacterial and antioxidant properties.

Beyond the appropriate mechanical strength [3], electrical conductivity [16] is the most important clinical requirement for cardiac patches that is mostly studied in the literature. However, antibacterial [17] and antioxidant [5] properties are additional desired characteristics of cardiac patches, which are also important to consider. Cardiac patches with antibacterial properties can mitigate bacterial growth at the site of surgery along with the reduction of inflammation [17]. Reduced inflammation following antibacterial or anti-inflammatory effects can decrease post-surgical adhesion complications [18, 19]. Moreover, increased reactive oxygen species [20] post-infarction makes the antioxidant cardiac patch a desired scaffold for myocardial regeneration [5]. The crucial role of selenium in antioxidant defense mechanisms for preventing cardiovascular diseases has been revealed before [20-27]. The antibacterial, antioxidant, and anti-inflammatory effects of selenium nanoparticles (SeNPs) have been reported in previous studies for biomedical applications [28, 29] such as myocardial regeneration because of their conductivity and antioxidant properties [30-32]. In addition, CS as a polysaccharide cationic polymer has been favorable for tissue engineering due to its non-toxicity, biodegradability, and biocompatibility properties [33-35] which is more favorable for cardiac tissue engineering due to its angiogenesis effects [30, 35, 36]. Furthermore, the CS-coated SeNPs (CS-SeNPs) exhibit antibacterial, antioxidant, and antiviral features [29, 37], that eligible them as a potent therapeutic strategy for myocardial infarction. In addition, the capacity of high drug loading of SeNPs with antioxidant and anti-inflammatory properties can introduce them as drug carrier [38, 39] to the site of myocardium infarction [40].

Different fabrication methods such as solvent casting, gas foaming, freeze-drying, electrospinning, and bioprinting are introduced to prepare a tissue-engineered scaffold [9], and each has its advantages and disadvantages. The electrospinning technique applies different polymers in various solvents that produces submicron nanofibers for mimicking the extracellular matrix [41].

In this study, an electrospun nanofiber cardiac patch containing Cs-SeNPs with antioxidant and antibacterial properties was fabricated to patch an infarcted myocardium in the rat model. To the best of our knowledge, the therapeutic potential of PCL/Cs-SeNPs nanofibers has not been investigated before in animal models of myocardial infarction *in vivo*.

MATERIALS AND METHODS

Chemicals, bacterial strains, and mammalian cells

The chemicals of sodium selenite (Na_2SeO_3, Sigma- Aldrich, USA), CS (low molecular weight, Sigma- Aldrich, USA), ascorbic acid (VC,

Shanghai, China), polycaprolactone (PCL, Mw 80,000, Hangzhou Ruijiang Chemical CO., Ltd, China), tetrahydrofuran (THF, Merck), methanol (CH3OH, 99.9%, Merck Chemicals, Germany), diphenylpicrylhydrazyl (DPPH) (C18H12N5O6, Sigma- Aldrich, USA), DMEM-F12 (GIBCO/BRL Invitrogen, Carlsbad, California), trypsin (Biosera, England), penicillin-streptomycin (Biosera, England), fetal bovine serum (FBS) (GIBCO/BRL Invitrogen, Carlsbad, California), and methyl-thiazolyl diphenyltetrazolium bromide (MTT, 98%, Sigma-Aldrich, USA) were used without further purification and modification. Staphylococcus aureus (*S. aureus*) (ATCC 25923) as gram-positive and Escherichia coli (*E. Coli*) (ATCC 25922) as gram-negative bacteria were applied as standard bacterial strains. The mammalian cells of mouse embryonic fibroblasts (3T3) were used for in vitro studies.

CS-SeNPs synthesis and characterization

Ascorbic acid was used for the chemical reduction of Na_2SeO_3 in the presence of CS as a stabilizing and capping agent for the synthesis of CS-SeNPs, as reported in our previous study [29]. Na_2SeO_3 with a concentration of 50 mM was mixed with 1% CS solution in magnetic stirring condition for 10 min at room temperature. The reduction agent of 50 mM ascorbic acid was added drop by drop into the solution of Na_2SeO_3 and CS, along with vigorous magnetic stirring for about 30–60 min to complete the reaction. The appearance of orange color verified the CS-SeNPs formation. The final concentration of CS-SeNPs was adjusted to 1000 ppm with the addition of deionized water.

A spectrophotometer (Bio Aquarius CE 7250, United Kingdom) was used for recording UV–vis absorption spectra of Milli-Q water diluted Cs-SeNPs in a range of 200–700 nm . The hydrodynamic diameter of CS-SeNPs was evaluated by dynamic light scattering (DLS) using a scatteroscope (K-ONE Ltd, South Korea). Transmission electron microscopy (TEM) (Zeiss-EM10C-100 KV, Germany) was utilized for determining the size and morphology of CS-SeNPs.

CS-SeNP-loaded nanofibers synthesis and characterization

A 15% concentration of PCL in THF solvent was used for the synthesis of nanofibers composite enriched with CS-SeNPs (PCL/Cs-SeNPs). PCL was dissolved in THF via magnetic stirring at 250 rpm for 3 hr at room temperature. As the electrospinning solution of PCL in THF got clear, colloidal CS-SeNPs were added into this solution in a volume of 75 µL for each 1 ml of solution drop by drop with simultaneous stirring. Complete dispersion of CS-SeNPs in an electrospinning solution was achieved after 1 hr. The electrospinning solution was loaded in a 5 mL syringe and blunt-ended stainless-steel needle with a 21-gauge to be injected with a flow rate of 1 mL/hr. Electrospinning parameters set for voltage of 20 kV, 10 cm distance for injection position to collector, collector rotating speed at 500 rpm, and room temperature.

PCL/CS-SeNPs morphology

The morphology of PCL/ CS-SeNPs nanofibers was evaluated by field emission scanning electron microscopy (FESEM) (TESCAN MIRA3). A mini sputter coater (SC7620) was used to coat the scaffold with gold in thickness of 4.5 nm towards a conductive surface for FESEM imaging.

ATR-FTIR analysis

Attenuated total reflectance–Fourier transform infrared (ATR–FTIR) spectroscopic (Tensor 27 Equinox 55) was used to obtain the ATR–FTIR spectra of PCL, CS, CS-SeNPs and PCL/CS-SeNPs over the range of 400-4000 cm^{-1}.

Mechanical test

A uniaxial tensile test was used to determine the mechanical properties of dry and wet PCL/ Cs-SeNPs (24 hr immersion in PBS (pH:7.4, 37°C)) for wet PCL/CS-SeNPs) in rectangular strips of 1×4 cm^2 (n≥3). The crosshead speed of 5 mm/min with Instron 5566 was used for stretching (load cell of 50N and gauge width of 15 mm).

Water contact angle

The hydrophilicity of nanofibers cardiac patches was evaluated with an OCA 15 plus device (Data Physics, Germany) to measure the water contact angle. PCL/CS-SeNPs and PCL nanofibers cardiac patches (n≥3) were fixed on the microscope slides and 4 µL drops of deionized water were placed on the surface. The images of drops were analyzed via Image J contact angle (Drop Analysis).

Antibacterial assessment

Viable cell count assessment was applied for evaluating the antibacterial properties of PCL/CS-SeNPs in direct exposure to *S. aureus* and *E. Coli*

bacteria with Spread Plate Counting [42] (n≥3).

Antioxidant assay (DPPH)

The antioxidant activity of the PCL/CS-SeNP nanofibers patch was evaluated with a DPPH radical scavenging assay [43] (n≥3). For the stock solution, 20 mg of DPPH was dissolved into 50 mL of methanol. Patches with an average weight of 10 mg were prepared in triplicates for each time point and were immersed into 3.75 mL of methanol in vials. The control sample was prepared in a vial containing 3.75 mL of methanol. Excluding the control vial, 0.25 mL of DPPH stock solution was added into each prepared vial, followed by incubating at 37 °C /100 rpm (orbital shaker). The absorbance of samples was measured at 517 nm for time points of 5, 15, 30, 60, 90, and 120 min. The antioxidant activity of samples was computed according to the following equation:

Evaluation of cell cytotoxicity with MTT assay

Mouse fibroblast 3T3 cells were used for evaluation of the cytotoxicity of PCL/CS-SeNPs and PCL nanofibers (n≥3) at 1, 3, 5, and 7 days. A puncher was used to prepare the round samples of electrospun PCL/CS-SeNPs and PCL for 96 well plates. Triplicate samples of each nanofiber patch were incubated with cells; 3 empty wells were determined as blank for each plate. Exposure to UV irradiation was used for sterilizing all plates, including nanofiber patches for 20 minutes for each side of patches. About 2000 cells were seeded on the scaffolds which were deposited into the wells and the culture medium changed every two days. At each time point, the whole medium was discarded from the wells and replaced with 200 µL of serum-free medium containing 25 µL of MTT (5%). The absorbance of samples was evaluated after 15 min of MTT exposure with shaking on a plate shaker by an ELISA reader at 570 nm.

Cell adhesion and morphology

SEM imaging was used to evaluate the cell attachment and cell morphology on the surface of nanofibers scaffolds. Nanofibers scaffolds of PCL/CS-SeNPs and PCL were cut into pieces for 24-well plates and sterilized with exposure to UV light for 20 min for each side of patches. About 10000 3T3 cells were seeded onto each well over the nanofibers scaffolds. Cell-seeded scaffolds were fixed after 3 days with formaldehyde 4% (20 min) following dehydration via increasing gradient of ethanol (35%, 50%, 70%, 80%, 90%, 100%). Gold-palladium coating was used to prepare the fixed samples for SEM imaging. In addition, DAPI/Phalloidin staining was used to evaluate the morphology of cultured cells over the nanofibers scaffolds. Triton X-100 in a concentration of 0.1% for 5 min was used to permeabilize the cell membrane for DAPI/Phalloidin staining.

In vivo animal model

NIH Guidelines for the Care and Use of Laboratory Animals (NIH Publication No. 85e23, revised 2010) were considered as a reference for all animal experiments. 20 male Wistar rats, weighing 300 -350 g, were evaluated in 4 groups (PCL/CS-SeNPs, PCL, Control, Sham) for this experiment. Separately, standard cages were used for animal housing under the standard condition; light-dark cycles of 12/12 h, 25 °C, 60% humidity, and free access to food and water. Intramuscular injections of Medetomidine (1 mg/kg, Syva, Spain) and ketamine (50 mg/kg, Alfasan, The Netherlands) were used to anesthetize the animals. Intubation of animals was performed with an angiocatheter (16G). The surgery area was shaved and disinfected with povidone-iodine. After left thoracotomy (third intercostal space), the pericardium was removed to expose the left ventricle (LV). Permanent ligation of left anterior descending artery (LAD) was performed with 5–0 monofilament silk suture material (Keyhan Teb, Iran) towards the acute myocardial infarction that appeared visually with cyanosis and dyskinesia at the time of surgery. Sham group underwent the same surgery without the LAD ligation. Nanofibers cardiac patches of PCL/CS-SeNP and PCL groups were sutured onto the infarcted site with three or four sutures. After the process of surgery, anesthesia reversion was performed with an intramuscular injection of Atipamezole (0.5 mg/kg, Syva, Spain). Prophylactic antibiotic of cefazolin (15 mg/kg) and analgesic of tramadol (20 mg/kg) were prescribed for 3 days post-surgery.

Echocardiography was performed for the 1st and 28th day post-surgery to evaluate the cardiac function. The echocardiographic findings that were measured and compared within groups of this study included the Ejection Fraction (EF) and Fractional shortening (FS). The EF indicates the blood volume pumped out by the left ventricle in each contraction and the FS indicates the size reduction in the left ventricle in the systole, that reported in percentage.

Also, Hematoxylin and eosin (H&E) and Masson trichrome (MT) staining were used for investigating the histological changes between

Table 1. Scoring system for post-surgical adhesion grading

Description	Score
Extent	
No involvement	0
s25% site involved	1
>25% but s50% site involved	2
>50% but s75% site involved	3
>75% site involved	4
Type	
None	0
Filmy, transparent, avascular	1
Opaque, translucent, avascular	2
Opaque, capillaries present	3
Opaque, larger vessels present	4
Tenacity	
None	0
Adhesions fall apart	1
Adhesions lysed with traction	2
Adhesions sharply dissected	3

different study groups. The extent of post-surgery adhesion was evaluated with the scoring system of Honey et al. [44] based on the characteristics of extent, type, and tenacity of adhesions (Table 1).

Statistical analysis

All data was performed on at least 3 samples and expressed as the mean ± standard deviation (SD). T-test and One-way ANOVA were used for statistical analysis. The statistical significance was considered as $P < 0.05$.

RESULTS

CS-SeNP synthesis and characterization

Chemical reduction of Na_2SeO_3 by ascorbic acid was used to synthesize the CS-SeNPs in the presence of CS as a stabilizer and capping agent. The colorless solution of Na_2SeO_3 was converted into an orange color via CS-SeNPs synthesis. The synthesis of CS-SeNPs led to the appearance of a peak at 249 nm in the UV-visible spectrum (Fig. 1). TEM imaging revealed the round shape morphology and size distribution of 51.2±2.43 nm for CS-SeNPs; however, the hydrodynamic diameter of CS-SeNPs was estimated about 194 nm via DLS (Fig. 1). This finding is in line with previously reported studies, which declared that the hydrodynamic diameter of different nanoparticles showed a larger diameter in DLS compared to TEM and SEM imaging [45, 46].

This discrepancy in the size of nanoparticles characterized by DLS toward TEM and SEM is affected by the surface characteristics of particles that absorb the solvent molecules on their surface. Differences in capping or stabilizer agents along with the different fabrication methods determine the surface characteristics and hydrodynamic diameter [45]; however, TEM and SEM imaging can reveal naked nanoparticle size and detailed

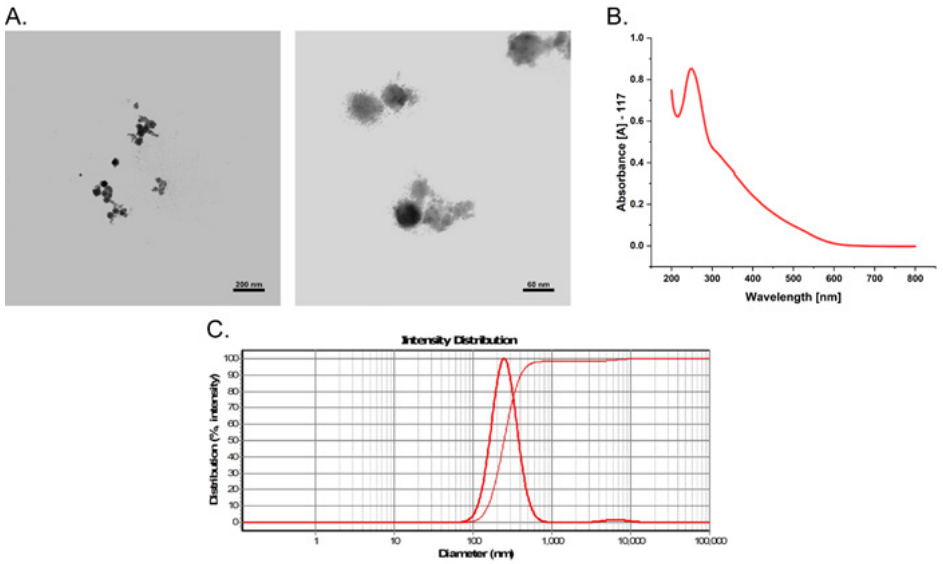

Fig 1. Characteristic tests for CS-SeNPs; A) TEM imaging showed CS-SeNPs with a round shape and size distribution of 51.2±2.43 nm (TEM images with scale bare of 200 nm and 60 nm), B) UV-visible spectroscopy showed a peak around 249 nm for CS-SeNPs, and C) The hydrodynamic diameter of CS-SeNPs investigated about 194 nm by DLS

analysis of the morphology of nanoparticles.

PCL/CS-SeNPs nanofibers synthesis and characterization

The electrospinning technique was used to fabricate fine nanofibers of PCL/CS-SeNPs. The FESEM images of PCL/CS-SeNPs showed the nanofibers with an average diameter of 648.36±259.19 nm with deposited CS-SeNPs (Fig. 2. A, B). The elemental Se in CS-SeNPs is also presented in EDX mapping (Fig. 2. C).

ATR-FTIR analysis

The ATR-FTIR spectrum of PCL/CS-SeNPs, PCL, CS, and CS-SeNPs is indicated in Fig. 3. A. The main ATR-FTIR characteristics of PCL are due to the bonds of asymmetric CH2, symmetric CH2, C=O, and C-O-C with presented peaks at 2938 cm^{-1}, 2865 cm^{-1}, 1637 cm^{-1}, and 1188 cm^{-1}. However, the ATR-FTIR characteristics of CS and CS-SeNPs are not well defined in PCL/CS-SeNPs due to very low concentration.

Mechanical test

The mechanical characteristics of PCL/CS-SeNPs cardiac patch in wet and dry status (n≥3) are reported in Fig. 3. B. The Young's modulus, tensile strength, and failure strain decreased in wet

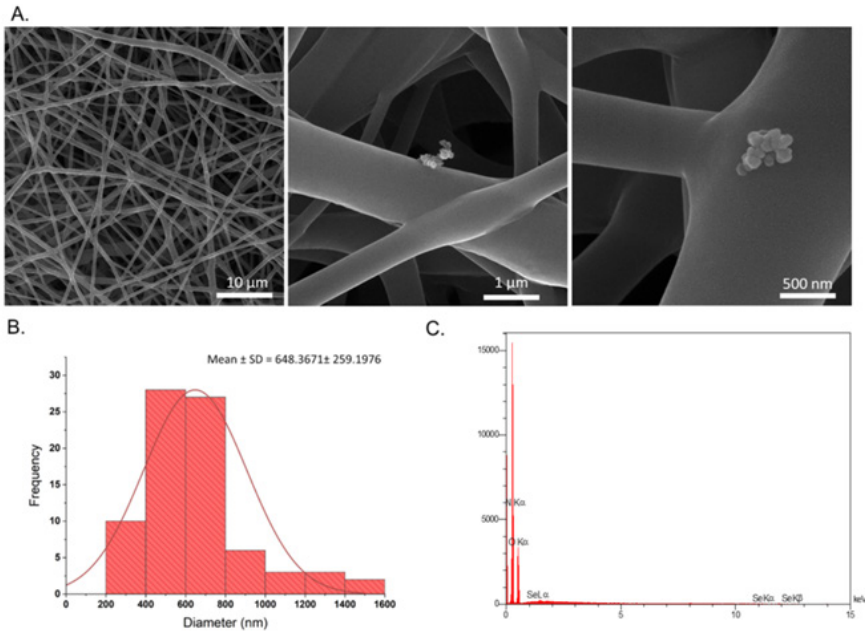

Fig. 2. Morphology and structural characteristics of PCL/CS-SeNPs nanofibers; A) FESEM imaging in magnifications of 10 µm, 1 µm, and 500 nm, B) Representative diagram for size distribution of PCL/CS-SeNPs nanofibers with average diameter of 648.36±259.19 nm, and C) Elemental composition of PCL/CS-SeNPs nanofibers in EDX for elemental Se identification

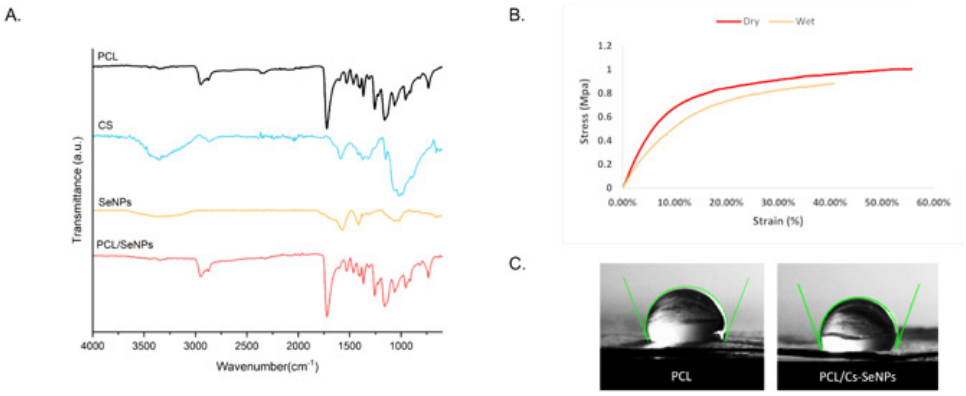

Fig. 3. A) ATR-FTIR analysis for PCL, CS, SeNPs, and PCL/CS-SeNPs nanofibers, B) Stress-strain characteristics for PCL/CS-SeNPs nanofibers in dry and wet conditions (n≥3), C) Decreased water contact angle of 124±3° in PCL nanofibers to 105.3±3.5° in PCL/CS-SeNPs nanofibers (n≥3).

Table 2. Mechanical properties of PCL/CS-SeNPs nanofibers in dry and wet conditions.

Type	Young's modulus	Tensile strength	Failure strain
Dry	9.4584±2.0318 Mpa	1.0055±0.0670 Mpa	55.72±1.543 %
Wet	5.7082±4.8547 Mpa	0.8819±0.0773 Mpa	40.78±3.190 %

patches in comparison to dry ones, as mentioned in Table 2. According to this fact that Young's modulus of native myocardium is about 0.02–0.5 MPa [30], the result of mechanical properties of PCL/Cs-SeNPs cardiac patch with Young's modulus of 5.7082±4.8547 MPa can be admissible for suture the infarcted myocardia.

Water contact angle

In hydrophobicity assessment, the water contact angle of PCL nanofibers cardiac patches decreased with the addition of CS-SeNPs into nanofibers of PCL/CS-SeNPs by 19% (124±3° to 105.3±3.5°) (Fig. 3. C) (n≥3).

Antibacterial assessment

Exposure of PCL/CS-SeNPs into gram-positive (*S. aureus*) and gram-negative (*E. coli*) bacteria by the viable cell count assessment revealed the proper antibacterial properties of this CS-SeNPs loaded cardiac patch. Viable cell count encountered with 60% and 50% reduction via one-hour exposure to PCL/CS-SeNPs and continued by 90% and 80% in 6 hours' exposure followed by 95% and 80% for 24 hr for gram-positive and gram-negative bacteria, respectively (Fig. 4. A).

Antioxidant assay (DPPH)

Fig. 4. B showed the antioxidant activity of PCL/CS-SeNPs patches by the DPPH assay in 5, 15, 30, 60, 90, and 120 min. Antioxidant activity of the patches reported about 27% within 120 min.

Evaluation of cell cytotoxicity with MTT assay

3T3 cells were used to evaluate the cell viability with MTT assay for 1, 3, 5, and 7 days. For the first

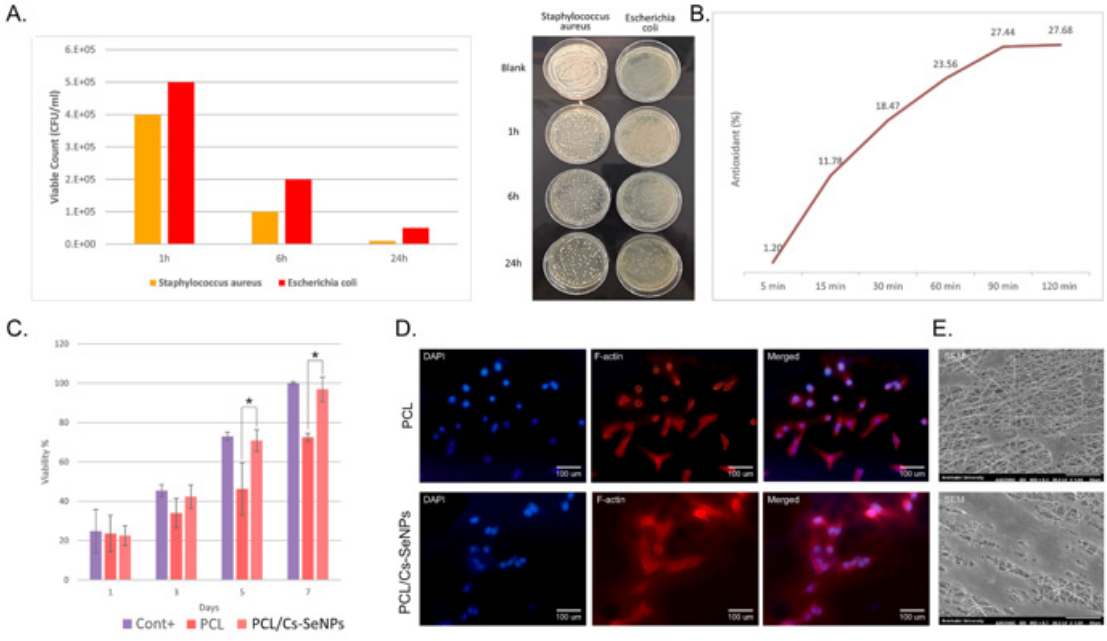

Fig 4. *In vitro* characteristics; A) Antibacterial effects of PCL/CS-SeNPs nanofibers after 1, 6, and 24 h evaluated by Viable cell count assay, and B) DPPH antioxidant assay reported the antioxidant properties of PCL/CS-SeNPs nanofibers within 120 min, C) Increased cell viability for 3T3 cells seeded on PCL/CS-SeNPs nanofibers observed at MTT Cytotoxicity assay, (n≥3) D) DAPI/Phalloidin staining for cytoskeleton of 3T3 cultured on PCL and PCL/CS-SeNPs nanofibers, E) SEM imaging of 3T3 cultured on PCL and PCL/CS-SeNPs nanofibers at 3rd day.

day, cell viability was not significantly different between groups of control and PCL and PCL/CS-SeNPs (P: 0.930). The viable cell count at day 7 was significantly different between PCL/CS-SeNPs and PCL cardiac patches (P: 0.003), though this difference for PCL/CS-SeNPs and control was not significant (P: 0.239) (Fig. 4. C).

Cell adhesion and morphology

Cell attachment of cultured 3T3 cells on the PCL and PCL/CS-SeNPs scaffolds after 3 days is exhibited in Fig. 4. E. Cell adhesion and expansion of 3T3 cells were improved on the scaffolds of PCL/CS-SeNPs compared to the PCL scaffold. The improved cell attachment of 3T3 cells on PCL/CS-SeNPs in comparison to the PCL scaffold can be due to the increased hydrophilicity [47] along with the antioxidant activity [48] of PCL/CS-SeNPs. DAPI/Phalloidin staining after 3 days represented the well-expanded cytoskeleton with improved cell-cell interactions and proliferation of 3T3 cells on the PCL/CS-SeNPs scaffolds compared to the PCL scaffolds (Fig. 4. D).

In vivo assessment

Myocardial infarcted rats were treated with suturing cardiac patches of PCL and PCL/CS-SeNPs scaffolds (Fig 5. A). PCL/Cs-SeNPs nanofibers decreased the postsurgical adhesion at day 28 post-MI. Three parameters were evaluated as extent, type, and tenacity of adhesions to surrounding tissues which indicated the reduction of total score of tissue adhesion to 52% for the PCL/SeNPs group compared to the PCL group (Fig 5. B, C).

Echocardiography results on day 28 after surgery revealed the improved function of the heart for the PCL/SeNPs group of study in comparison with PCL and Sham groups (Fig 6. A, C, D). EF for PCL/CS-SeNPs and PCL groups were

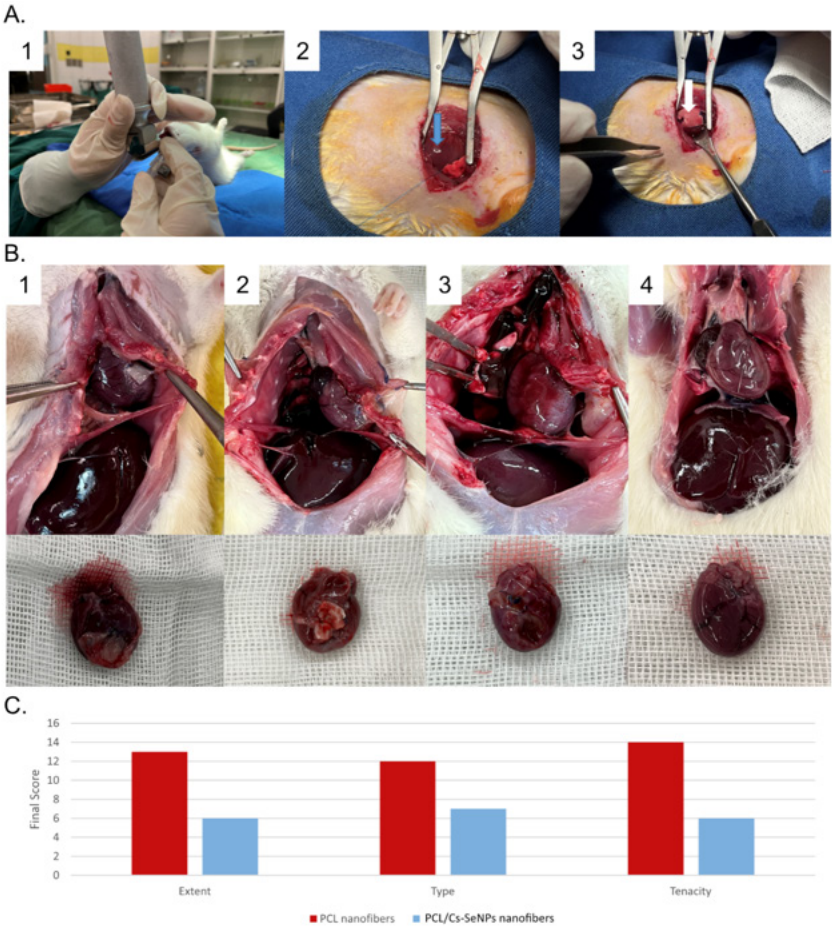

Fig 5. A) *In vivo* MI model in the rat; (1) Intubation, (2) LAD ligation, (3) Cardiac patch suturing, B) Exposing the surgery sites on the 28th day for post-surgical adhesion evaluation; (1) PCL/CS-SeNPs, (2) PCL, (3) MI, and (4) control, C) Decreased post-surgical adhesion reported by quantification and scoring system

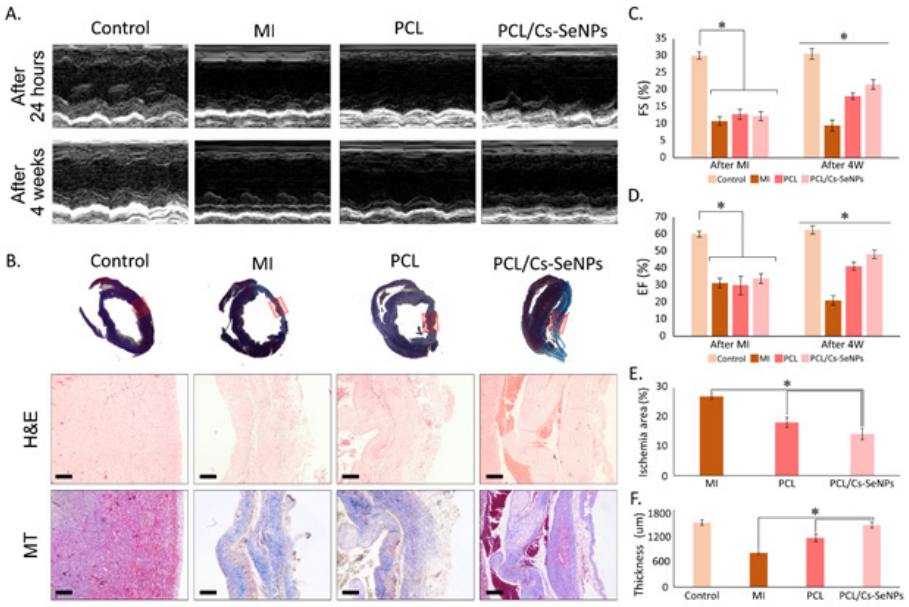

Fig 6. Echocardiographic and histopathological characteristics; A, C, D) The echocardiography at 24 hr and 4 weeks after MI revealed improved cardiac function via EF and FS measures, B) H&E and MT staining for 4 weeks after MI, E, F) Quantification of the ischemic area and left ventricular thickness at 4th-week post-MI supported the decreased ischemic area along with increased ventricular thickness at 4th weeks after MI for PCL/Cs-SeNPs nanofibers

significantly different compared to the sham group after 28 days (55.30± 2.75% and 46.63± 0.54% for PCL/CS-SeNPs and PCL versus 62.60± 0.0.86% and 24.13± 1.20% for control and Sham groups, respectively), that were also reflected in positive values of FS (25.06± 1.43% and 20.33± 0.33% for PCL/Cs-SeNPs and PCL versus 29.8± 0.32% and 9.53± 0.47% for control and Sham groups, respectively). The histological findings disclosed that functional restoration of myocardia in PCL/CS-SeNPs and PCL groups was associated with the lower fibrotic tissue formation, shown by MT staining of the left ventricular wall (Fig. 6. B). Quantification of histopathological images in the different groups supported the decreased ischemic area along with increased wall thickness of LV in the PCL/CS-SeNPs group (Fig. 6. E, F).

DISCUSSION

Cardiac tissue engineering aims to decrease the mortality rate of cardiovascular diseases and generally complies with three main principles of tissue engineering; scaffolds, cells, and small molecules [2, 4]. Different kinds of materials were used for the construction of cardiac patches, which mostly rely on mechanical properties and electrical conductivity [2, 4, 16, 43]. The induced conductivity to cardiac patches with PPy, PANI, poly(3,4-ethylenedioxythiophene) doped with polystyrene sulfonate (PEDOT:PSS), gold nanomaterials, and carbon nanomaterials has been reported by various studies [49-53]. Though most studies focused on the conductivity properties of cardiac patches, other determinant characteristics for myocardial rehabilitation have been recently considered, such as antioxidant and antibacterial effects [5, 17, 54-59]. Carvalho et al. [43] designed an antioxidant and anti-inflammatory cardiac patch constructed of lysozyme nanofibrils (LNFs)/ curcumin incorporated in gelatin electrospun nanocomposite. The addition of 5% w/w of LNFs increased the antioxidant effects of this cardiac patch by 80% and decreased the degradation rate to 30-35 days in comparison to 45 days of the gelatin-only patch. The drug release of curcumin resulted in a 15% burst release following a prolonged release of 21 days. However, this study lacks *in vivo* investigations. Shiekh et al. designed another antioxidant cardiac patch by incorporating ascorbic acid as a natural antioxidant into the polymeric backbone of polyurethane [59]. This antioxidant cardiac patch improved the cell proliferation for C2C12 mouse myoblasts and H9C2 rat cardiomyoblasts in comparison to the control group. In this study, a significant reduction in intracellular oxidative stress in H9C2 cardiomyoblasts was reported as a promising approach for the reduction of ischemic reperfusion-

induced cell death. Baheiraei et al. [56] designed an electroactive construct with antioxidant properties for cardiac tissue engineering applications with a blend of polyurethane and aniline pentamer with PCL. This antioxidant bio-electroactive blend supported the desired cell proliferation and attachment for L929 mouse fibroblast and human umbilical vein endothelial cells (HUVECs). Another antioxidant hydrogel cardiac patch was designed by Zuluaga et al. [58] that used polyvinyl alcohol/ dextran to deliver astaxanthin as an antioxidant agent to reduce the generation of myofibril stress after MI. Cell viability of 3T3 cells and HUVEC with biocompatibility evaluation supported the positive effects of this tissue-engineered construct for potential cardiac patches. Broadly, cardiac patches with antioxidant properties have been beneficial for cardiac regeneration after myocardial infarction.

Besides, the antioxidant properties of cardiac patches, antibacterial activity is another desired property to patch the infarcted myocardial. Norahan et al. used a coating of reduced graphene oxide on the collagen scaffolds for designing a conductive and antibacterial cardiac patch. The improved cell viability of HUVEC cultured on this scaffold along with upregulated expression in cardiac-specific genes of Cx43, Troponin-T, and actinin-4 was observed [60]. Talebi et al. [17] used polypyrrole in a construct of Cs-PCL to develop another conductive and antibacterial cardiac patch. Polypyrrole in the concentration of 7.5% led to increased conductivity of CS-PCL from 0.0164±0.008 to 0.55±0.03 mS/m. In addition, the polypyrrole-containing film exhibited increased antibacterial properties against *S. aureus* and *E. coli*. Another study was performed by Sauvage et al. [53] to fabricate an antibacterial and conductive cardiac patch based on PEDOT:PSS and PVA. This construct of PEDOT:PSS-PVA exhibited high electrical conductivity of 40 S/cm and an antibacterial effect against S. aureus.

Se element, a trace element, is present in the form of selenocysteine and selenomethionine in the selenoproteins of the human body, making it essential for the activity of many enzymes [61]. IT has been introduced by previous studies as an effective element for preventing cardiovascular diseases as a ROS scavenging agent [30, 62, 63]. Different *in vitro* and *in vivo* studies reported the protective effects of SeNPs on cardiomyoblasts, cardiomyocytes, and cardiovascular health [6, 23, 54]. Following the benefits of SeNPs for myocardial regeneration, Kalishwaralal et al. produced a CS nanocomposite film incorporated with SeNPs as a cardiac patch. This SeNPs loaded nanocomposite exhibited conductivity of 0.0055 S/cm with a tensile strength of 419 kPa, and supported the cell attachment and proliferation of the H9C2 cell line [30]. However, the antioxidant and antibacterial effects of this film were not evaluated. In the case of cardiac patch designing, CS presented angiogenesis properties besides improved conductivity, immunomodulatory effects, cell proliferation, and differentiation which are desired for cardiac regeneration. In addition to cardiac scaffold fabrication, CS has been applied to deliver drugs, cells, and growth factors at the site of infarction [30, 35, 36]. However, the degradation rate of CS is not favorable enough to provide the desired mechanical properties as a cardiac patch, CS is mostly used in combination with other natural [34] or synthetic materials [35, 64]. Moreover, it is applied as a stabilizer and capping agent for different nanoparticle syntheses such as palladium nanoparticles [65], gold nanoparticles [66], silk fibroin nanoparticles [67], and silver nanoparticles [68, 69]. Following the supportive findings over the protective effects of antioxidant and antibacterial agents for myocardial regeneration after MI, besides the desired effects of CSfor cardiac regeneration, a PCL/CS-SeNPs nanofibers scaffold was designed in this study.

Several studies designed SeNPs-loaded nanofibers for different biomedical applications (Table 3), though no study perused this construct as a nanofiber cardiac patch for cardiac regeneration. Chung et al. used the physisorption of SeNPs (in diameters of 40 and 70 nm) into the electrospun silk nanofibers (in diameters about 100-200 nm) to fabricate SeNPs-loaded nanofibers. The presence of SeNPs on silk nanofibers led to improved cell activity of human dermal fibroblasts, besides decreased ATP activity of *S. aureus* [70]. Doostmohammadi et al. loaded the SeNPs and vitamin E to PCL/Gelatin nanofibers for wound dressing application. *In vitro* studies revealed that the presence of SeNPs in the PCL/Gelatin nanofibers led to increased 3T3 cell viability and attachment. *In vivo* study in wound healing model supported the superiority of SeNPs containing nanofibers in complete re-epithelialization and low inflammatory response [71]. Furthermore, as Se is an essential element for selenoproteins in the body, there is no concern about the release of SeNPs in the body

Table 3. SeNPs loaded nanofibers in the different studies

Polymer/concentration	Solvent	SeNPs	Fiber diameter	Results	Ref
PCL (94%)	THF/DMF	- 0.6% w/v - Adding to polymer solution	~ 350 nm	- Reduced hydrophobicity	(73)
PCL (NM)	THF/DMF	- 0.2%, 0.4%, 0.6%, 0.8% w/v - 1% w/v - Adding to electrospinning solution	~ 100- 200 nm ~ 200- 300 nm	- Increased bead formation following increasing SeNPs concentration	(74)
Silk (8%)	Formic acid	- Physisorption of the SeNPs (40 and 70 nm) onto the silk scaffold	~ 100- 200 nm	- Improved cell activity - Reduced ATP activity in S. aureus bacteria	(70)
β-(1→3)-D-glucan polysaccharide (self-assemble hollow nanofibers)	DW	- Physisorption of the SeNPs (46 nm)	~ 193 nm	- Enhanced cellular uptake - Synergetic anti-cancer effect - Cell apoptosis and cell cycle arrest *in vitro* MCF-7 cells - Anti-tumor effects *in vivo*	(75)
PCL/Gel (15%/10%)	Acetic acid 80%	- Adding to polymer solution (80–220 nm) plus Vitamin E	~ 397.82 nm	- Decreased contact angle - Enhanced cell viability - Increased GSH levels of tissues treated - Decreased MDA levels - Improved wound healing *in vivo*	(71)

in therapeutic doses. In addition, the potential of these nanoparticles for drug delivery and gene delivery has been investigated in previous studies which makes it worth considering this nanoparticle as a therapeutic approach [72]. According to the results, PCL/CS-SeNPs nanofibers with antioxidant and antibacterial properties represented a potential cardiac patch to improve heart function along with reduced post-surgical adhesion.

CONCLUSION

In the present study, a SeNPs-loaded nanofiber (PCL/Cs-SeNPs) was developed as a cardiac patch with antioxidant and antibacterial properties. The PCL/Cs-SeNPs nanofibers with an average diameter of 648.36±259.19 nm showed the preserved antioxidant and antibacterial effects of Cs-SeNPs incorporated into PCL nanofibers. No cytotoxicity was observed in the MTT assay for PCL/Cs-SeNPs nanofiber scaffold. Enhanced cell adhesion was investigated for 3T3 cells seeded on PCL/Cs-SeNPs nanofibers in comparison with PCL nanofibers. Improved cardiac function via increased EF and FS along with the reduced post-surgical adhesion was observed with PCL/Cs-SeNPs cardiac patch in the in-vivo study of the MI model in rats in comparison with PCL nanofibers alone. The presence of antibacterial and antioxidant Cs-SeNPs with low toxicity in the nanofiber introduces this scaffold as a potent carrier for drug delivery systems to the infarcted myocardium for future studies.

ACKNOWLEDGMENTS

The present research has been supported by the Tehran University of Medical Sciences (Grant number: 40569-223-01-98).

CONFLICTS OF INTEREST

The authors declare no conflict of interest.

REFERENCES

1. Shahabadi N, Zendehcheshm S, Khademi F. Selenium nanoparticles: Synthesis, in-vitro cytotoxicity, antioxidant activity and interaction studies with ct-DNA and HSA, HHb and Cyt c serum proteins. Biotechnol Rep (Amst). 2021;30:e00615.
2. Boroumand S, Haeri A, Nazeri N, Rabbani S. Review Insights In Cardiac Tissue Engineering: Cells, Scaffolds, and Pharmacological Agents. Iran J Pharm Res. 2021;20(4):467-496.
3. Li M, Wu H, Yuan Y, Hu B, Gu N. Recent fabrications and applications of cardiac patch in myocardial infarction treatment. View. 2022;3(2):20200153.
4. Mei X, Cheng K. Recent Development in Therapeutic Cardiac Patches. Front Cardiovasc Med. 2020;7:610364.
5. Carvalho T, Ezazi NZ, Correia A, Vilela C, Santos HA, Freire CS. Gelatin-Lysozyme Nanofibrils Electrospun Patches with Improved Mechanical, Antioxidant and Bioresorbability Properties for Myocardial Regeneration Applications. Adv Funct Mater. 2022:2113390.
6. Kalishwaralal K, Jeyabharathi S, Sundar K, Muthukumaran A. Sodium selenite/selenium nanoparticles (SeNPs) protect cardiomyoblasts and zebrafish embryos against ethanol induced oxidative stress. J Trace Elem Med Biol. 2015;32:135-144.
7. Mei X, Cheng K. Recent development in therapeutic cardiac patches. Front Cardiovasc Med. 2020;7:610364.
8. Nazari H, Heirani-Tabasi A, Esmaeili E, Kajbafzadeh AM, Hassannejad Z, Boroomand S, et al. Decellularized human amniotic membrane reinforced by MoS(2)-Polycaprolactone nanofibers, a novel conductive scaffold for cardiac tissue engineering. J Biomater Appl. 2022;36(9):1527-1539.
9. Sigaroodi F, Rahmani M, Parandakh A, Boroumand S, Rabbani S, Khani M-M. Designing cardiac patches for myocardial regeneration–a review. Int J Polym Mater. 2024;73(7):581-599.
10. Mondal D, Griffith M, Venkatraman SS. Polycaprolactone-

based biomaterials for tissue engineering and drug delivery: Current scenario and challenges. Int J Polym. Mater. 2016;65:255-265.
11. Vogt L, Rivera LR, Liverani L, Piegat A, El Fray M, Boccaccini AR. Poly (ε-caprolactone)/poly (glycerol sebacate) electrospun scaffolds for cardiac tissue engineering using benign solvents. Mater Sci Eng C Mater Biol Appl. 2019;103:109712.
12. Rai R, Tallawi M, Frati C, Falco A, Gervasi A, Quaini F, et al. Bioactive electrospun fibers of poly (glycerol sebacate) and poly (ε-caprolactone) for cardiac patch application. Adv Healthc Mater. 2015;4(13):2012-2025.
13. Spearman BS, Hodge AJ, Porter JL, Hardy JG, Davis ZD, Xu T, et al. Conductive interpenetrating networks of polypyrrole and polycaprolactone encourage electrophysiological development of cardiac cells. Acta Biomater. 2015;28:109-120.
14. Yang Y, Lei D, Huang S, Yang Q, Song B, Guo Y, et al. Elastic 3D-Printed Hybrid Polymeric Scaffold Improves Cardiac Remodeling after Myocardial Infarction. Adv Healthc Mater. 2019;8(10):e1900065.
15. He Y, Ye G, Song C, Li C, Xiong W, Yu L, et al. Mussel-inspired conductive nanofibrous membranes repair myocardial infarction by enhancing cardiac function and revascularization. Theranostics. 2018;8(18):5159-5177.
16. Ashtari K, Nazari H, Ko H, Tebon P, Akhshik M, Akbari M, et al. Electrically conductive nanomaterials for cardiac tissue engineering. Adv Drug Deliv Rev. 2019;144:162-179.
17. Talebi A, Labbaf S, Karimzadeh F. A conductive film of chitosan-polycaprolcatone-polypyrrole with potential in heart patch application. Polym Test. 2019;75:254-261.
18. Fatehi Hassanabad A, Zarzycki AN, Jeon K, Dundas JA, Vasanthan V, Deniset JF, et al. Prevention of post-operative adhesions: a comprehensive review of present and emerging strategies. Biomolecules. 2021;11(7):1027.
19. Boroumand S, Hosseini S, Salehi M, Faridi Majidi R. Drug-loaded electrospun nanofibrous sheets as barriers against postsurgical adhesions in mice model. Nanomed Res J. 2017;2(1):64-72.
20. Benstoem C, Goetzenich A, Kraemer S, Borosch S, Manzanares W, Hardy G, et al. Selenium and its supplementation in cardiovascular disease—what do we know? Nutrients. 2015;7(5):3094-3118.
21. Dasgupta S, Aly AM. Dilated cardiomyopathy induced by chronic starvation and selenium deficiency. Case Rep Pediatr. 2016;2016.
22. Zhang X, Liu C, Guo J, Song Y. Selenium status and cardiovascular diseases: meta-analysis of prospective observational studies and randomized controlled trials. Eur J Clin Nutr. 2016;70(2):162-169.
23. Kalishwaralal K, Jeyabharathi S, Sundar K, Muthukumaran A. Comparative analysis of cardiovascular effects of selenium nanoparticles and sodium selenite in zebrafish embryos. Artif Cells Nanomed Biotechnol. 2016;44(3):990-996.
24. Alehagen U, Aaseth J, Johansson P. Reduced cardiovascular mortality 10 years after supplementation with selenium and coenzyme Q10 for four years: follow-up results of a prospective randomized double-blind placebo-controlled trial in elderly citizens. PloS one. 2015;10(12):e0141641.
25. Flores-Mateo G, Navas-Acien A, Pastor-Barriuso R, Guallar E. Selenium and coronary heart disease: a meta-analysis. Am J Clin Nutr. 2006;84(4):762-773.
26. Xiao S, Mao L, Xiao J, Wu Y, Liu H. Selenium nanoparticles inhibit the formation of atherosclerosis in apolipoprotein E deficient mice by alleviating hyperlipidemia and oxidative stress. Eur J Pharmacol. 2021;902:174120.
27. Shimada BK, Alfulaij N, Seale LA. The Impact of Selenium Deficiency on Cardiovascular Function. Int J Mol Sci. 2021;22(19).
28. El-Ghazaly M, Fadel N, Rashed E, El-Batal A, Kenawy S. Anti-inflammatory effect of selenium nanoparticles on the inflammation induced in irradiated rats. Can J Physiol Pharmacol. 2017;95(2):101-110.
29. Boroumand S, Safari M, Shaabani E, Shirzad M, Faridi-Majidi R. Selenium nanoparticles: synthesis, characterization and study of their cytotoxicity, antioxidant and antibacterial activity. Mater Res Express. 2019;6(8):0850d8.
30. Kalishwaralal K, Jeyabharathi S, Sundar K, Selvamani S, Prasanna M, Muthukumaran A. A novel biocompatible chitosan–Selenium nanoparticles (SeNPs) film with electrical conductivity for cardiac tissue engineering application. Mater Sci Eng C Mater Biol Appl. 2018;92:151-160.
31. Naveenkumar S, Venkateshan N, Kaviyarasu K, Christyraj JRSS, Muthukumaran A. Optimum performance of a novel biocompatible scaffold comprising alginate-pectin-selenium nanoparticles for cardiac tissue engineering using C2C12 cells. J Mol Struct. 2023;1294:136457.
32. Abbas MM, Abdelmonem HA, Mahmoud AH. Prophylactic Effect of Costus and Selenium Nanoparticles in Isoproterenol Induced Myocardial Infarction in Rats. Egypt J Hosp Med. 2022;89(1):4817-4823.
33. Chen S, Tian H, Mao J, Ma F, Zhang M, Chen F, et al. Preparation and application of chitosan-based medical electrospun nanofibers. Int J Biol Macromol. 2023;226:410-422.
34. Chen J, Zhan Y, Wang Y, Han D, Tao B, Luo Z, et al. Chitosan/silk fibroin modified nanofibrous patches with mesenchymal stem cells prevent heart remodeling post-myocardial infarction in rats. Acta Biomater. 2018;80:154-168.
35. Kazemi Asl S, Rahimzadegan M, Ostadrahimi R. The recent advancement in the chitosan hybrid-based scaffolds for cardiac regeneration after myocardial infarction. Carbohydr Polym. 2023;300:120266.
36. Patel B, Manne R, Patel DB, Gorityala S, Palaniappan A, Kurakula M. Chitosan as Functional Biomaterial for Designing Delivery Systems in Cardiac Therapies. Gels. 2021;7(4):253.
37. Boroumand S, Majidi RF, Gheibi A, Majidi RF. Selenium nanoparticles incorporated in nanofibers media eliminate H1N1 activity: a novel approach for virucidal antiviral and antibacterial respiratory mask. Environ Sci Pollut Res Int. 2024;31(2):2360-2376.
38. Karthik K, Cheriyan BV, Rajeshkumar S, Gopalakrishnan M. A review on selenium nanoparticles and their biomedical applications. Biomed. Technol. 2024;6:61-74.
39. Lin W, Zhang J, Xu J-F, Pi J. The advancing of selenium nanoparticles against infectious diseases. Front Pharmacol. 2021;12:682284.
40. George TA, Hsu CC, Meeson A, Lundy DJ. Nanocarrier-Based Targeted Therapies for Myocardial Infarction. Pharmaceutics. 2022;14(5).
41. Zulkifli MZA, Nordin D, Shaari N, Kamarudin SK. Overview of Electrospinning for Tissue Engineering Applications. Polymers (Basel). 2023;15(11).
42. Huang CL, Lee KM, Liu ZX, Lai RY, Chen CK, Chen WC, et al. Antimicrobial Activity of Electrospun Polyvinyl Alcohol Nanofibers Filled with Poly[2-(tert-butylaminoethyl)

Methacrylate]-Grafted Graphene Oxide Nanosheets. Polymers (Basel). 2020;12(7).
43. Carvalho T, Ezazi NZ, Correia A, Vilela C, Santos HA, Freire CS. Gelatin-lysozyme nanofibrils electrospun patches with improved mechanical, antioxidant, and bioresorbability properties for myocardial regeneration applications. Adv Funct Mater. 2022;32(21):2113390.
44. Haney A, Hesla J, Hurst BS, Kettel LM, Murphy AA, Rock JA, et al. Expanded polytetrafluoroethylene (Gore-Tex Surgical Membrane) is superior to oxidized regenerated cellulose (Interceed TC7) in preventing adhesions. Fertil Steril. 1995;63(5):1021-1026.
45. Boroumand S, Majidi RF, Gheibi A, Majidi RF. Selenium nanoparticles incorporated in nanofibers media eliminate H1N1 activity: a novel approach for virucidal antiviral and antibacterial respiratory mask. ESPR. 2024;31(2):2360-76.
46. Jia Z, Li J, Gao L, Yang D, Kanaev A. Dynamic Light Scattering: A Powerful Tool for In Situ Nanoparticle Sizing. Colloids Interfaces. 2023;7(1):15.
47. Ehtesabi H, Massah F. Improvement of hydrophilicity and cell attachment of polycaprolactone scaffolds using green synthesized carbon dots. Mater. Today Sustain. 2021;13:100075.
48. Li J, Fang W, Hao T, Dong D, Yang B, Yao F, et al. An anti-oxidative and conductive composite scaffold for cardiac tissue engineering. Compos B Eng. 2020;199:108285.
49. Liang Y, Mitriashkin A, Lim TT, Goh JC-H. Conductive polypyrrole-encapsulated silk fibroin fibers for cardiac tissue engineering. Biomaterials. 2021;276:121008.
50. Cui Z, Ni NC, Wu J, Du G-Q, He S, Yau TM, et al. Polypyrrole-chitosan conductive biomaterial synchronizes cardiomyocyte contraction and improves myocardial electrical impulse propagation. Theranostics. 2018;8(10):2752.
51. Yin Q, Zhu P, Liu W, Gao Z, Zhao L, Wang C, et al. A Conductive Bioengineered Cardiac Patch for Myocardial Infarction Treatment by Improving Tissue Electrical Integrity. Adv Healthc Mater. 2023;12(1):e2201856.
52. Liu W, Zhao L, Wang C, Zhou J. Conductive nanomaterials for cardiac tissues engineering. Engineered Regeneration. 2020;1:88-94.
53. Sauvage E, Matta J, Dang CT, Fan J, Cruzado G, Cicoira F, et al. Electroconductive cardiac patch based on bioactive PEDOT:PSS hydrogels. J Biomed Mater Res A. 2024; 112(10):1817-1826.
54. Yang X, SAN LOON K, Fu Y, Liu J, Peng Y, Zhang J, et al. Selenium nanoparticles reduce cardiomyocyte apoptosis in Ascites Syndrome in Broiler Chickens via the ATF6-DR5 signaling pathway. Anim Dis. 2023; 22 (3).
55. Norahan MH, Pourmokhtari M, Saeb MR, Bakhshi B, Zomorrod MS, Baheiraei N. Electroactive cardiac patch containing reduced graphene oxide with potential antibacterial properties. Mater Sci Eng C Mater Biol Appl. 2019;104:109921.
56. Baheiraei N, Yeganeh H, Ai J, Gharibi R, Azami M, Faghihi F. Synthesis, characterization and antioxidant activity of a novel electroactive and biodegradable polyurethane for cardiac tissue engineering application. Mater Sci Eng C Mater Biol Appl. 2014;44:24-37.
57. Mahmoudi M, Zhao M, Matsuura Y, Laurent S, Yang PC, Bernstein D, et al. Infection-resistant MRI-visible scaffolds for tissue engineering applications. BioImpacts: BI. 2016;6(2):111.
58. Zuluaga M, Gregnanin G, Cencetti C, Di Meo C, Gueguen V, Letourneur D, et al. PVA/Dextran hydrogel patches as delivery system of antioxidant astaxanthin: A cardiovascular approach. Biomedical Materials. 2017;13(1):015020.
59. Shiekh PA, Singh A, Kumar A. Engineering bioinspired antioxidant materials promoting cardiomyocyte functionality and maturation for tissue engineering application. ACS Appl Mater Interfaces. 2018;10(4):3260-3273.
60. Norahan MH, Pourmokhtari M, Saeb MR, Bakhshi B, Soufi Zomorrod M, Baheiraei N. Electroactive cardiac patch containing reduced graphene oxide with potential antibacterial properties. Mater Sci Eng C Mater Biol Appl. 2019;104:109921.
61. Hariharan S, Dharmaraj S. Selenium and selenoproteins: It's role in regulation of inflammation. Inflammopharmacology. 2020;28(3):667-695.
62. Ojeda ML, Sobrino P, Rua RM, Gallego-Lopez MdC, Nogales F, Carreras O. Selenium, a dietary-antioxidant with cardioprotective effects, prevents the impairments in heart rate and systolic blood pressure in adolescent rats exposed to binge drinking treatment. Am J Drug Alcohol Abuse. 2021;47(6):680-693.
63. Al-Mubarak AA, van der Meer P, Bomer N. Selenium, selenoproteins, and heart failure: current knowledge and future perspective. Curr Heart Fail Rep. 2021;18(3):122-131.
64. Ahmadi P, Nazeri N, Derakhshan MA, Ghanbari H. Preparation and characterization of polyurethane/chitosan/CNT nanofibrous scaffold for cardiac tissue engineering. Int J Biol Macromol. 2021;180:590-598.
65. Phan TTV, Hoang G, Nguyen VT, Nguyen TP, Kim HH, Mondal S, et al. Chitosan as a stabilizer and size-control agent for synthesis of porous flower-shaped palladium nanoparticles and their applications on photo-based therapies. Carbohydr Polym. 2019;205:340-352.
66. Franconetti A, Carnerero JM, Prado-Gotor R, Cabrera-Escribano F, Jaime C. Chitosan as a capping agent: Insights on the stabilization of gold nanoparticles. Carbohydr Polym. 2019;207:806-814.
67. Collado-González M, Montalbán MG, Peña-García J, Pérez-Sánchez H, Víllora G, Díaz Baños FG. Chitosan as stabilizing agent for negatively charged nanoparticles. Carbohydr Polym. 2017;161:63-70.
68. Laghrib F, Houcini H, Khalil F, Liba A, Bakasse M, Lahrich S, et al. Synthesis of Silver Nanoparticles Using Chitosan as Stabilizer Agent: Application towards Electrocatalytical Reduction of p-Nitrophenol. ChemistrySelect. 2020;5(3):1220-1227.
69. Costa M, Carreiro EP, Filho CM, Silva M, Gonçalves I, Souza EF, et al. Chitosan Salts as Stabilizing Agents for the Synthesis of Silver Nanoparticles (AgNPs). ChemistrySelect. 2023;8(1):e202203413.
70. Chung S, Ercan B, Roy AK, Webster TJ. Addition of Selenium Nanoparticles to Electrospun Silk Scaffold Improves the Mammalian Cell Activity While Reducing Bacterial Growth. Front Physiol. 2016;7:297.
71. Doostmohammadi M, Forootanfar H, Shakibaie M, Torkzadeh-Mahani M, Rahimi HR, Jafari E, et al. Bioactive anti-oxidative polycaprolactone/gelatin electrospun nanofibers containing selenium nanoparticles/vitamin E for wound dressing applications. J Biomater Appl. 2021;36(2):193-209.
72. Karthik KK, Cheriyan BV, Rajeshkumar S, Gopalakrishnan M. A review on selenium nanoparticles and their biomedical applications. Biomed. Technol. 2024;6:61-74.
73. Kamaruzaman NA, Yusoff ARM, Malek N, Talib M. Fabrication, characterization and degradation of electrospun

poly (ε-caprolactone) infused with selenium nanoparticles. Malays J Fundam Appl Sci. 2021;17:295-305.
74. Kamaruzaman NA, Yusoff ARM, Buang NA, Salleh NGN, editors. Effects on diameter and morphology of polycaprolactone nanofibers infused with various concentrations of selenium nanoparticles. AIP Conference Proceedings; 2017: AIP Publishing.
75. Ping Z, Liu T, Xu H, Meng Y, Li W, Xu X, et al. Construction of highly stable selenium nanoparticles embedded in hollow nanofibers of polysaccharide and their antitumor activities. Nano Research. 2017;10:3775-3789.